Excited bottom-charmed mesons in a nonrelativistic quark model

Qi Li, Ming-Sheng Liu, Long-Sheng Lu, Qi-Fang Lü,* Long-Cheng Gui,† and Xian-Hui Zhong‡

Department of Physics, Hunan Normal University, Changsha 410081, China, Synergetic Innovation Center for Quantum Effects and Applications (SICQEA), Changsha 410081, China and Key Laboratory of Low-Dimensional Quantum Structures and Quantum Control of Ministry of Education, Changsha 410081, China

(Received 1 April 2019; published 22 May 2019)

Using the newly measured masses of $B_c(1S)$ and $B_c(2S)$ from the CMS Collaboration and the $1S$ hyperfine splitting determined from the lattice QCD as constraints, we calculate the B_c mass spectrum up to the $6S$ multiplet with a nonrelativistic linear potential model. Furthermore, using the wave functions from this model we calculate the radiative transitions between the B_c states within a constituent quark model. For the higher mass B_c states lying above DB threshold, we also evaluate the Okubo-Zweig-Iizuka (OZI) allowed two-body strong decays with the $^3P_0$ model. Our study indicates that there is large potential for the observations of the low-lying B_c states below the DB threshold via their radiative transitions; in addition, some higher mass B_c states, such as $B_c(2^3P_2)$, $B_c(2^3D_1)$, $B_c(3^3D_1)$, $B_c(4^3P_0)$, and the $1F$-wave B_c states, might be first observed in their dominant strong decay channels DB, DB^*, or D^*B at the LHC for their relatively narrow widths.

DOI: 10.1103/PhysRevD.99.096020

I. INTRODUCTION

The B_c states are composed of a bottom-charmed quark-antiquark pair, as an important family of hadron spectra was predicted in theory about 40 years ago [1]; however, the experimental progress towards establishing the B_c spectrum is not obvious. Except for the ground state B_c meson observed in 1998 by the CDF Collaboration at Fermilab [2], until 2018, only the ATLAS Collaboration reported evidence of an excited B_c state with a mass of 6842 ± 9 MeV [3] consistent with the values predicted for $B_c(2S)$, while it was not confirmed by the LHCb Collaboration by using their 8 TeV data sample [4]. The poor situation of the observations and measurements of the B_c spectrum is due to the production yields being significantly smaller than those of the charmonium and bottomonium ($c\bar{c}$ and $b\bar{b}$) states. Fortunately, the LHC provides good opportunities for our search for the excited B_c states with its high collision energies and integrated luminosity. Very recently, two excited B_c^+ states were observed in the $B_c^+\pi^+\pi^-$ invariant mass spectrum by the CMS Collaboration [5]. Signals are consistent with the $B_c(2S)$ and $B_c^*(2S)$ states. These two states are well resolved from each other and are observed with a significance exceeding five standard deviations. The mass of the $B_c(2S)$ meson, 6871 ± 2.8 MeV, measured by the CMS Collaboration is inconsistent with the determination 6842 ± 9 MeV by the ATLAS Collaboration. The reason is that the peak observed by ATLAS could be the superposition of the $B_c(2S)$ and $B_c^*(2S)$ states, too closely spaced with respect to the resolution of the measurement [5].

The B_c states as the only conventional heavy mesons with different flavors have aroused great interest in theory. Compared with the $c\bar{c}$ and $b\bar{b}$ spectra, the B_c spectrum has several special features for the bottom-charmed quark-antiquark pair. (i) The B_c states cannot annihilate into gluons; thus, the low-lying excited B_c states below the DB threshold are more stable with a narrow width less than a few hundred keV, and they mainly decay via the electromagnetic or hadronic transitions between two different B_c states. (ii) In the B_c meson spectrum there are configuration mixings between the states with different total spins but with the same total angular momentum, such as $^3P_1 - {}^1P_1$, $^3D_2 - {}^1D_2$, and $^3F_3 - {}^1F_3$ mixings via the antisymmetric part of the spin-orbit potential. (iii) Additionally, the B_c states provide a unique window for studying the heavy-quark dynamics that is very different from those provided by the $c\bar{c}$ and $b\bar{b}$ states. In the past years, the B_c mass spectrum has been predicted with various models [6–34]. Furthermore, a few lattice calculations can be found in Refs. [35–39]. To estimate the production rates in experiments, the production of the excited B_c states was often

*lvqifang@hunnu.edu.cn
†guilongcheng@hunnu.edu.cn
‡zhongxh@hunnu.edu.cn

discussed in the literature [40–53]. As the dominant decay modes, the electromagnetic transitions of the low-lying B_c states were also widely estimated in the literature [7–16, 54–58]. However, the studies of the Okubo-Zweig-Iizuka (OZI)-allowed strong decays for the high-lying B_c states are confined only to a few calculations [17,18,59,60].

The successes of the observations of the radially excited B_c states $B_c(2S)$ and $B_c^*(2S)$ by the CMS Collaboration [5] have demonstrated that more excited B_c states are to be discovered in future LHC experiments. Stimulated by the great discovery potentials of the missing B_c states in future experiments, in the present work we carry out a systematic study of the B_c spectrum. First, using the newly measured masses of $B_c(1S)$ and $B_c(2S)$ from the CMS Collaboration [5] and the $1S$ hyperfine splitting determined from the lattice QCD [36–38] as constraints, we calculate the B_c mass spectrum up to the $6S$ multiplet with a nonrelativistic linear potential model. The slope parameter of the linear potential has been well determined in our previous study of the charmonium states [61]. To involve the spin-dependent corrections of the spatial wave functions, following the method adopted in Refs. [61,62], we treat the spin-dependent interactions as nonperturbative terms in our calculations. With this nonperturbative treatment, we can reasonably include the effect of spin-dependent interactions on the spatial wave functions, which is essential for us to gain reliable predictions of the decay behaviors.

Then, with the available wave functions from the potential model, we evaluate the electromagnetic (EM) transitions between the B_c states within a nonrelativistic constituent quark model developed in our previous works [61,62]. With this approach, the possible higher EM multipole contributions to an EM transition process can be included naturally. Considering the fact that the higher B_c states lying above the DB threshold may have enough possibilities to be produced at LHC, and they are easy to be established in the $D^{(*)}B^{(*)}$ hadronic final states, thus, to give useful references for the LHC observations, we further calculate the OZI-allowed strong decays of the higher B_c states within the widely used $^3P_0$ model [63–65]. It is found that $B_c(2^3P_2)$, $B_c(^3D_1)$, $B_c(3^3D_1)$ together with the $1F$-wave B_c states might be first observed in their dominant strong decay channels DB, DB^*, or D^*B at LHC for their relatively narrow width.

This paper is organized as follows. In Sec. II, the B_c mass spectrum is calculated within a nonrelativistic linear potential model. Then, with the obtained B_c spectrum the radiative transitions between the B_c states are estimated in Sec. III within a nonrelativistic constituent quark model. In Sec. IV, the OZI-allowed two-body strong decays of the excited B_c state are also studied within the $^3P_0$ model. In Sec. V, we focus on the calculation results and discuss some strategies for looking for the B_c states in future experiments. Finally, a summary is given in Sec. VI.

II. MASS SPECTRUM

To describe a bottom-charmed meson system, we adopt a nonrelativistic linear potential model. In this model, the effective quark-antiquark potential is written as the sum of the spin-independent term $H_0(r)$ and spin-dependent term $H_{sd}(r)$; i.e.,

$$V(r) = H_0(r) + H_{sd}(r), \tag{1}$$

where

$$H_0(r) = -\frac{4}{3}\frac{\alpha_s}{r} + br \tag{2}$$

includes the standard color Coulomb interaction and the linear confinement. The spin-dependent part $H_{sd}(r)$ can be expressed as [1,9,11]

$$H_{sd}(r) = H_{SS} + H_T + H_{LS}, \tag{3}$$

where

$$H_{SS} = \frac{32\pi\alpha_s}{9m_q m_{\bar{q}}}\tilde{\delta}_\sigma(r)\mathbf{S}_q\cdot\mathbf{S}_{\bar{q}} \tag{4}$$

is the spin-spin contact hyperfine potential. Here, we take $\tilde{\delta}_\sigma(r) = (\sigma/\sqrt{\pi})^3 e^{-\sigma^2 r^2}$ as suggested in Ref. [66]. The tensor potential H_T is adopted as

$$H_T = \frac{4}{3}\frac{\alpha_s}{m_q m_{\bar{q}}}\frac{1}{r^3}\left(\frac{3\mathbf{S}_q\cdot\mathbf{r}\mathbf{S}_{\bar{q}}\cdot\mathbf{r}}{r^2} - \mathbf{S}_q\cdot\mathbf{S}_{\bar{q}}\right). \tag{5}$$

For convenience in the calculations, the potential of the spin-orbit interaction H_{LS} is decomposed into symmetric part $H_{\rm sym}$ and antisymmetric part $H_{\rm anti}$,

$$H_{LS} = H_{\rm sym} + H_{\rm anti}, \tag{6}$$

with

$$H_{\rm sym} = \frac{\mathbf{S}_+\cdot\mathbf{L}}{2}\left[\left(\frac{1}{2m_{\bar{q}}^2} + \frac{1}{2m_q^2}\right)\left(\frac{4}{3}\frac{\alpha_s}{r^3} - \frac{b}{r}\right) + \frac{8\alpha_s}{3m_q m_{\bar{q}} r^3}\right], \tag{7}$$

$$H_{\rm anti} = \frac{\mathbf{S}_-\cdot\mathbf{L}}{2}\left(\frac{1}{2m_q^2} - \frac{1}{2m_{\bar{q}}^2}\right)\left(\frac{4}{3}\frac{\alpha_s}{r^3} - \frac{b}{r}\right). \tag{8}$$

In these equations, $\mathbf{L}$ is the relative orbital angular momentum of the $q\bar{q}$ system; $\mathbf{S}_q$ and $\mathbf{S}_{\bar{q}}$ are the spins of the quark q and antiquark $\bar{q}$, respectively, and $\mathbf{S}_\pm \equiv \mathbf{S}_q \pm \mathbf{S}_{\bar{q}}$; m_q and $m_{\bar{q}}$ are the masses of quark q and antiquark $\bar{q}$, respectively; α_s is the running coupling constant of QCD; and r is the distance between the quark q and antiquark $\bar{q}$.

The five parameters in the above equations (α_s, b, σ, m_b, m_c) are determined by fitting the spectrum.

We can get the masses and wave functions by solving the radial Schrödinger equation,

$$\frac{d^2u(r)}{dr^2}+2\mu_R\left[E-V_{q\bar{q}}(r)-\frac{L(L+1)}{2\mu_R r^2}\right]u(r)=0, \quad (9)$$

with

$$V_{q\bar{q}}(r)=V(r)+H_{SS}+H_{SL}+H_T, \quad (10)$$

where $\mu_R=m_q m_{\bar{q}}/(m_q+m_{\bar{q}})$ is the reduced mass of the system, and E is the binding energy of the system. Then, the mass of a bottom-charmed state is obtained by

$$M_{q\bar{q}}=m_q+m_{\bar{q}}+E. \quad (11)$$

In this work, to reasonably include the corrections from these spin-dependent potentials to both the mass and wave function of a meson state, we deal with the spin-dependent interactions nonperturbatively. We solve the radial Schrödinger equation by using the three-point difference central method [67] from central ($r=0$) towards outside ($r\to\infty$) point by point. This method was successfully to deal with the spectroscopies of $c\bar{c}$ and $b\bar{b}$ [61,62]. To overcome the singular behavior of $1/r^3$ in the spin-dependent potentials, following the method of our previous works [61,62], we introduce a cutoff distance r_c in the calculation. Within a small range $r\in(0,r_c)$, we let $1/r^3=1/r_c^3$.

Finally, it should be mentioned that the antisymmetric part of the spin-orbit potential, H_{anti}, can let the states with different total spins but with the same total angular momentum, such as $B_c(n^3L_J)$ and $B_c(n^1L_J)$, mix with each other. Thus, as mixing states between $B_c(n^3L_J)$ and $B_c(n^1L_J)$, the physical B_c states $B_c(nL)$ and $B_c(nL')$ are expressed as

$$\begin{pmatrix} B_c(nL'_J) \\ B_c(nL_J) \end{pmatrix}=\begin{pmatrix} \cos\theta_{nL} & \sin\theta_{nL} \\ -\sin\theta_{nL} & \cos\theta_{nL} \end{pmatrix}\begin{pmatrix} B_c(n^1L_J) \\ B_c(n^3L_J) \end{pmatrix}, \quad (12)$$

where $J=L=1,2,3\cdots$, and the θ_{nL} is the mixing angle. In this work $B_c(nL')$ corresponds to the higher mass mixed state as often adopted in the literature.

In this work the parameter set is taken as $\alpha_s=0.5021$, $b=0.1425$ GeV^2, $m_b=4.852$ GeV, $m_c=1.483$ GeV, $\sigma=1.3$ GeV, and $r_c=0.16$ fm. To be consistent with our previous study [61], the charmed quark mass m_c and the slope for the linear confining potential are taken from the determinations, i.e., $m_c=1.483$ GeV and $b=0.1425$ GeV^2. The other three parameters (m_b, α_s, σ) are determined by fitting the masses of the B_c, B_c^*, and $B_c(2S)$ mesons. The masses of B_c and $B_c(2S)$ are taken from the recent measurements of the CMS Collaboration [5]. Although the B_c^* meson is still not measured in experiments, the mass difference between the B_c^* and B_c is predicted to be around 55 MeV from lattice QCD [36–38]. Thus, combining it with the measured mass 6271 MeV for B_c, in present work we estimate the mass of B_c^* as $\sim$6326 MeV. The cutoff distance r_c is determined by the mass of $B_c(1^3P_0)$. To determine the mass of $B_c(1^3P_0)$, we adopt a method of perturbation; i.e., we let $H=H_0+H'$, where H' is a part which contains the term of $1/r^3$. By solving the equation of $H_0|\psi_n^{(0)}\rangle=E_0|\psi_n^{(0)}\rangle$, we can get the energy E_0 and wave function $|\psi_n^{(0)}\rangle$; then, we obtain the mass of $B_c(1^3P_0)$, $M=m_b+m_c+E_0+\langle\psi_n^{(0)}|H'|\psi_n^{(0)}\rangle$.

By solving the radial Schrödinger equation and with the determined parameter set, we obtain the masses of the bottom-charmed states, which have been listed in Table I and shown in Fig. 1. For comparison, the other model predictions in Refs. [7–11,15,16] are listed in the same table as well.

It is found that the masses of the low-lying $1S$-, $2S$-, $3S$-, $1P$-, $2P$-, $1D$-wave B_c states predicted in this work are compatible with the other potential model predictions. For the higher mass states, such as $4S$-, $5S$-, $6S$-, $3P$-, $4P$-, $2D$-, $2F$-, $3F$-wave states, the masses predicted by us are very close to those predicted with a relativistic model in Ref. [8], while they are about 100–200 MeV smaller than those predicted in Refs. [15,16]. Furthermore, the hyperfine splitting between $B_c^*(2S)$ and $B_c(2S)$ is predicted to be 19 MeV, which is slightly smaller than 30–45 MeV, predicted in previous works [7–11,15,16,36–38]. Finally, it should be pointed out that the mixing angles for $^3P_1-{}^1P_1$, $^3D_2-{}^1D_2$, and $^3F_3-{}^1F_3$ have obvious model dependencies (see Table II).

III. RADIATIVE TRANSITIONS

We use the nonrelativistic constituent quark model as adopted in Refs. [61,62,68–72] to calculate the radiative transitions between the B_c states. In this model, the quark-photon EM coupling at the tree level is taken as

$$H_e=-\sum_j e_j\bar{\psi}_j\gamma_\mu^j A^\mu(\mathbf{k},\mathbf{r})\psi_j, \quad (13)$$

where A^μ represents the photon field with three momenta $\mathbf{k}$; while e_j and $\mathbf{r}_j$ stand for the charge and coordinate of the constituent quark ψ_j, respectively. In order to match the nonrelativistic wave functions of the B_c states, we adopt the nonrelativistic form of Eq. (13), which is given by [73–78]

$$H_e^{nr}=\sum_j\left[e_j\mathbf{r}_j\cdot\boldsymbol{\epsilon}-\frac{e_j}{2m_j}\boldsymbol{\sigma}_j\cdot(\boldsymbol{\epsilon}\times\hat{\mathbf{k}})\right]e^{-i\mathbf{k}\cdot\mathbf{r}_j}, \quad (14)$$

TABLE I. Predicted masses (MeV) of B_c states compared with other model predictions and data. The mixing angles between $B_c(n^3L_J)$ and $B_c(n^1L_J)$ obtained in this work are presented in Table II.

State	J^P	Ours	ZVR [8]	SJSCP [16]	MBV [15]	EQ [7]	EFG [10]	GI [11]	KLT [9]	Lattice [36]	Exp [5]
$B_c(1^3S_1)$	1^-	6326 (input)	6340	6321	6357	6337	6332	6338	6317	6331 ± 10	⋯
$B_c(1^1S_0)$	0^-	6271 (input)	6260	6272	6275	6264	6270	6271	6253	6276 ± 9	6271
$B_c(2^3S_1)$	1^-	6890	6900	6900	6897	6899	6881	6887	6902	⋯	⋯
$B_c(2^1S_0)$	0^-	6871 (input)	6850	6864	6862	6856	6835	6855	6867		6871
$B_c(3^3S_1)$	1^-	7252	7280	7338	7333	7280	7235	7272	⋯	⋯	⋯
$B_c(3^1S_0)$	0^-	7239	7240	7306	7308	7244	7193	7250	⋯	⋯	⋯
$B_c(4^3S_1)$	1^-	7550	7580	7714	7734	7594	⋯	⋯	⋯	⋯	⋯
$B_c(4^1S_0)$	0^-	7540	7550	7684	7713	7562	⋯	⋯	⋯	⋯	⋯
$B_c(5^3S_1)$	1^-	7813	⋯	8054	8115	⋯	⋯	⋯	⋯	⋯	⋯
$B_c(5^1S_0)$	0^-	7805	⋯	8025	8097	⋯	⋯	⋯	⋯	⋯	⋯
$B_c(6^3S_1)$	1^-	8054	⋯	8368	8484	⋯	⋯	⋯	⋯	⋯	⋯
$B_c(6^1S_0)$	0^-	8046	⋯	8340	8469	⋯	⋯	⋯	⋯	⋯	⋯
$B_c(1^3P_2)$	2^+	6787	6760	6712	6737	6747	6762	6768	6743	⋯	⋯
$B_c(1P_1')$	1^+	6776	6740	⋯	6734	6736	6749	6750	6729	⋯	⋯
$B_c(1P_1)$	1^+	6757	6730	⋯	6686	6730	6734	6741	6717	6736 ± 24	⋯
$B_c(1^3P_0)$	0^+	6714	6680	6686	6638	6700	6699	6706	6683	6712 ± 25	⋯
$B_c(2^3P_2)$	2^+	7160	7160	7173	7175	7153	7156	7164	7134	⋯	⋯
$B_c(2P_1')$	1^+	7150	7150	⋯	7173	7142	7145	7150	7124	⋯	⋯
$B_c(2P_1)$	1^+	7134	7140	⋯	7137	7135	7126	7145	7113	⋯	⋯
$B_c(2^3P_0)$	0^+	7107	7100	7146	7084	7108	7091	7122	7088	⋯	⋯
$B_c(3^3P_2)$	2^+	7464	7480	7565	7575	⋯	⋯	⋯	⋯	⋯	⋯
$B_c(3P_1')$	1^+	7458	7470	⋯	7572	⋯	⋯	⋯	⋯	⋯	⋯
$B_c(3P_1)$	1^+	7441	7460	⋯	7546	⋯	⋯	⋯	⋯	⋯	⋯
$B_c(3^3P_0)$	0^+	7420	7430	7536	7492	⋯	⋯	⋯	⋯	⋯	⋯
$B_c(4^3P_2)$	2^+	7732	7760	7915	7970	⋯	⋯	⋯	⋯	⋯	⋯
$B_c(4P_1')$	1^+	7727	7740	⋯	7942	⋯	⋯	⋯	⋯	⋯	⋯
$B_c(4P_1)$	1^+	7710	7740	⋯	7943	⋯	⋯	⋯	⋯	⋯	⋯
$B_c(4^3P_0)$	0^+	7693	7710	7885	7970	⋯	⋯	⋯	⋯	⋯	⋯
$B_c(1^3D_3)$	3^-	7030	7040	6990	7004	7005	7081	7045	7134	⋯	⋯
$B_c(1D_2')$	2^-	7032	7030	⋯	7003	7012	7079	7036	7124	⋯	⋯
$B_c(1D_2)$	2^-	7024	7020	⋯	6974	7009	7077	7041	7113	⋯	⋯
$B_c(1^3D_1)$	1^-	7020	7010	6998	6973	7012	7072	7025	7088	⋯	⋯
$B_c(2^3D_3)$	3^-	7348	7370	7399	7410	⋯	⋯	⋯	⋯	⋯	⋯
$B_c(2D_2')$	2^-	7347	7360	⋯	7408	⋯	⋯	⋯	⋯	⋯	⋯
$B_c(2D_2)$	2^-	7343	7360	⋯	7385	⋯	⋯	⋯	⋯	⋯	⋯
$B_c(2^3D_1)$	1^-	7336	7350	7403	7377	⋯	⋯	⋯	⋯	⋯	⋯
$B_c(3^3D_3)$	3^-	7625	7660	7761	7796	⋯	⋯	⋯	⋯	⋯	⋯
$B_c(3D_2')$	2^-	7623	7650	⋯	7783	⋯	⋯	⋯	⋯	⋯	⋯
$B_c(3D_2)$	2^-	7620	7650	⋯	7781	⋯	⋯	⋯	⋯	⋯	⋯
$B_c(3^3D_1)$	1^-	7611	7640	7762	7761	⋯	⋯	⋯	⋯	⋯	⋯
$B_c(1^3F_4)$	4^+	7227	7250	7244	⋯	⋯	⋯	7271	⋯	⋯	⋯
$B_c(1F_3')$	3^+	7240	7250	⋯	⋯	⋯	⋯	7266	⋯	⋯	⋯
$B_c(1F_3)$	3^+	7224	7240	⋯	⋯	⋯	⋯	7276	⋯	⋯	⋯
$B_c(1^3F_2)$	2^+	7235	7240	7234	⋯	⋯	⋯	7269	⋯	⋯	⋯
$B_c(2^3F_4)$	4^+	7514	7550	7617	⋯	⋯	⋯	7568	⋯	⋯	⋯
$B_c(2F_3')$	3^+	7525	7550	⋯	⋯	⋯	⋯	7571	⋯	⋯	⋯
$B_c(2F_3)$	3^+	7508	7540	⋯	⋯	⋯	⋯	7563	⋯	⋯	⋯
$B_c(2^3F_2)$	2^+	7518	7540	7607	⋯	⋯	⋯	7565	⋯	⋯	⋯
$B_c(3^3F_4)$	4^+	7771	7810	7956	⋯	⋯	⋯	⋯	⋯	⋯	⋯
$B_c(3F_3')$	3^+	7779	7810	⋯	⋯	⋯	⋯	⋯	⋯	⋯	⋯
$B_c(3F_3)$	3^+	7768	7800	⋯	⋯	⋯	⋯	⋯	⋯	⋯	⋯
$B_c(3^3F_2)$	2^+	7730	7800	7946	⋯	⋯	⋯	⋯	⋯	⋯	⋯

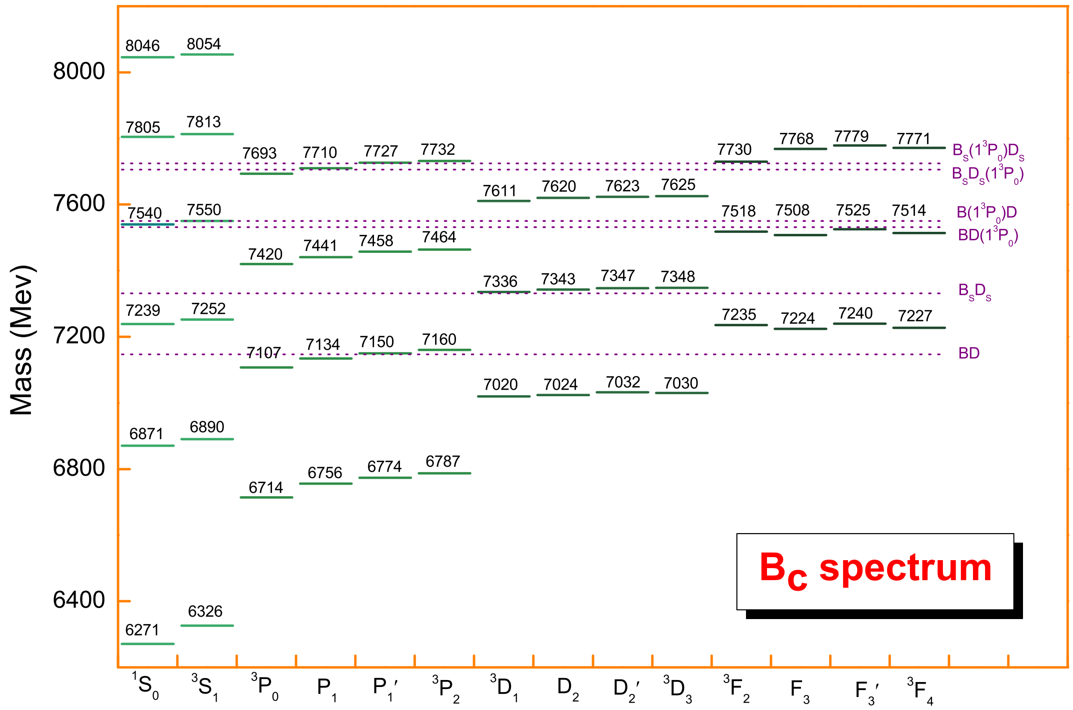

FIG. 1. The spectrum of B_c mesons.

where $\boldsymbol{\epsilon}$ is the polarization vector of the final photon, m_j and $\boldsymbol{\sigma}_j$ stand for the constituent mass and Pauli spin vector for the jth quark. The helicity amplitude $\mathcal{A}$ can be expressed as

$$\mathcal{A} = -i\sqrt{\frac{\omega_\gamma}{2}}\langle f|H_e^{nr}|i\rangle. \tag{15}$$

Finally, we obtain the partial decay width of a radiative transition by

$$\Gamma = \frac{|\mathbf{k}|^2}{\pi}\frac{2}{2J_i+1}\frac{M_f}{M_i}\sum_{J_{fz},J_{iz}}|\mathcal{A}_{J_{fz},J_{iz}}|^2, \tag{16}$$

where J_i is the total angular momentum of an initial meson, and J_{fz} and J_{iz} are the components of the total angular momenta along the z axis of initial and final mesons, respectively. M_i and M_f correspond to the masses of the initial and final B_c states, respectively.

The radiative decay properties for the B_c states have been listed in Tables III–VIII. For comparison, some other predictions of the low-lying B_c states from Refs. [7,9–11] are also given in the tables.

TABLE II. Mixing angles.

Mixing angle	Ours	[11]	[14]	[10]
θ_{1P}	35.5°	22.4°	20.57°	20.4°
θ_{2P}	38.0°	18.9°	19.94°	23.2°
θ_{3P}	39.7°	…	17.68°	…
θ_{4P}	39.7°	…	…	…
θ_{1D}	45.0°	44.5°	−2.49°	−35.9°
θ_{2D}	45.0°	…	−2.8°	…
θ_{3D}	45.0°	…	…	…
θ_{1F}	41.4°	41.4°	…	…
θ_{2F}	43.4°	…	…	…
θ_{3F}	42.4°	…	…	…

IV. STRONG DECAYS

In this work, we use the $^3P_0$ model [63–65] to calculate the OZI-allowed strong decays of the bottom-charmed

TABLE III. Partial widths of the $M1$ transitions for the low-lying $1S$-, $2S$-, and $3S$-wave B_c states compared with the other model predictions.

		E_γ (MeV)					Γ_{M1} (eV)				Γ_{M1} (eV)
Initial state	Final state	[7]	[10]	[11]	[9]	Ours	[7]	[10]	[11]	[9]	Ours
1^3S_1	1^1S_0	72	62	67	64	55	134.5	73	80	60	57
2^3S_1	2^1S_0	43	46	32	35	19	28.9	30	10	10	2.4
	1^1S_0	606	584	588	649	591	123.4	141	600	98	1205
2^1S_0	1^3S_1	499	484	498	550	523	93.3	160	300	96	99
3^3S_1	3^1S_0			22		13			3		0.8
	2^1S_0			405		371			200		356
	1^1S_0			932		915			600		1885
3^1S_0	2^3S_1			354		341			60		152
	1^3S_1			855		855			4200		510

TABLE IV. Partial widths of the $M1$ transitions for the higher nS-wave ($n = 4, 5, 6$) B_c states.

Initial state	Final state	E_γ (MeV)	$\Gamma_{\rm EM}$ (eV)	Initial state	Final state	E_γ (MeV)	$\Gamma_{\rm EM}$ (eV)
4^1S_0	3^3S_1	283	186	4^3S_1	4^1S_0	10	0.35
	2^3S_1	622	579		3^1S_0	305	252
	1^3S_1	1116	1122		2^1S_0	648	806
					1^1S_0	1171	2501
5^1S_0	4^3S_1	251	209	5^3S_1	5^1S_0	8	0.18
	3^3S_1	533	720		4^1S_0	268	210
	2^3S_1	861	1260		3^1S_0	553	675
	1^3S_1	1339	1893		2^1S_0	885	1316
					1^1S_0	1390	3107
6^1S_0	5^3S_1	230	225	6^3S_1	6^1S_0	8	0.18
	4^3S_1	481	849		5^1S_0	245	191
	3^3S_1	755	1613		4^1S_0	498	643
	2^3S_1	1073	2203		3^1S_0	774	1239
	1^3S_1	1536	2822		2^1S_0	1096	1917
					1^1S_0	1586	3772

mesons. In this model, it assumes that the vacuum produces a quark-antiquark pair with the quantum number 0^{++} and the heavy meson decay takes place via the rearrangement of the four quarks. The transition operator $\hat{T}$ in this model can be written as

$$\hat{T} = -3\gamma\sqrt{96\pi}\sum_m \langle 1m1-m|00\rangle \int d\mathbf{p}_3 d\mathbf{p}_4 \delta^3(\mathbf{p}_3+\mathbf{p}_4) \times \mathcal{Y}_1^m\left(\frac{\mathbf{p}_3-\mathbf{p}_4}{2}\right)\chi^{34}_{1-m}\phi^{34}_0\omega^{34}_0 b^\dagger_{3i}(\mathbf{p}_3)d^\dagger_{4j}(\mathbf{p}_4), \quad (17)$$

where γ is a dimensionless constant that denotes the strength of the quark-antiquark pair creation with momentum $\mathbf{p}_3$ and $\mathbf{p}_4$ from vacuum; $b^\dagger_{3i}(\mathbf{p}_3)$ and $d^\dagger_{4j}(\mathbf{p}_4)$ are the creation operators for the quark and antiquark, respectively; the subscriptions, i and j, are the SU(3)-color indices of the created quark and antiquark; $\phi^{34}_0 = (u\bar{u}+d\bar{d}+s\bar{s})/\sqrt{3}$ and $\omega^{34}_0 = \frac{1}{\sqrt{3}}\delta_{ij}$ correspond to flavor and color singlets, respectively; $\chi^{34}_{1,-m}$ is a spin triplet state; and

TABLE V. Partial widths of the $E1$ dominant radiative transitions for the $1P$-, $1D$-, and $1F$-wave B_c states. For comparison, the predictions from the relativistic quark model [10], relativized quark model [11], nonrelativistic constituent quark models [7,9] are listed in the table as well.

		E_γ (MeV)					$\Gamma_{\rm E1}$ (keV)				$\Gamma_{\rm EM}$ (keV)
Initial state	Final state	[7]	[10]	[11]	[9]	Ours	[7]	[10]	[11]	[9]	Ours
1^3P_2	1^3S_1	397	416	416	426	445	112.6	122	83	102.9	87
$1P'_1$		387	405	399	412	433	0.1	13.7	11	8.1	40
$1P_1$		382	389	391	400	416	99.5	87.1	60	77.8	70
1^3P_0		353	355	358	366	377	79.2	75.5	55	65.3	96
$1P'_1$	1^1S_0	455	463	462	476	484	56.4	147	80	131.1	74
$1P_1$		450	447	454	464	468	0	18.4	13	11.6	35
1^3D_3	1^3P_2	258	312	272	264	239	98.7	149	78	76.9	67
$1D'_2$	1^3P_2		310	263	273	241		12.6	8.8	6.8	8.3
	$1P'_1$		321	280	287	253		143	63	46.0	41
	$1P_1$		338	289	301	271		7.1	7	25.0	0.39
$1D_2$	1^3P_2		308	268	258	233		23.6	9.6	12.2	8.7
	$1P'_1$		319	285	272	246		14.9	15	18.4	1.09
	$1P_1$		335	294	284	263		139	64	44.6	44
1^3D_1	1^3P_2	258	303	255	265	229	2.7	3.82	1.8	2.2	0.7
	$1P'_1$	268	315	273	279	242	0	7.81	4.4	3.3	12
	$1P_1$	331	315	281	291	259	49.3	65.3	28	39.2	29
	1^3P_0	302	365	315	325	299	88.6	133	55	79.9	65
1^3F_4	1^3D_3			222		194			81		69
$1F'_3$	1^3D_3			227		207			5.4		4.76
	$1D'_2$			231		205			82		32
	$1D_2$			236		212			0.04		0.04
$1F_3$	1^3D_3			218		191			3.7		4.91
	$1D'_2$			222		189			0.5		0.22
	$1D_2$			226		197			78		29
1^3F_2	1^3D_3			221		202			0.4		0.12
	$1D'_2$			224		200			6.3		5.72
	$1D_2$			229		208			6.5		6.36
	1^3D_1			237		212			75		78

TABLE VI. Partial widths of the $E1$ dominant radiative transitions for the $2D$-wave B_c states.

Initial state	Final state	E_γ (MeV)	Γ_{EM} (keV)	Initial state	Final state	E_γ (MeV)	Γ_{EM} (keV)
2^3D_1	1^3P_2	528	8.13	2^3D_3	1^3P_2	540	32
	$1P'$	540	7.6		$1P'$	552	0.54
	$1P$	557	12.5		$1P$	568	1.23
	1^3P_0	596	41.8		1^3P_0	607	2.04
	2^3P_2	174	0.58		2^3P_2	186	54
	$2P'$	184	10.15		$2P'$	195	0.09
	$2P$	199	20.88		$2P$	211	0.23
	2^3P_0	225	46		2^3P_0	237	0.05
$2D_2$	1^3P_2	535	7.04	$2D_2'$	1^3P_2	539	7.28
	$1P'$	547	0.12		$1P'$	551	19
	$1P$	564	22.6		$1P$	567	1.48
	1^3P_0	602	0.29		1^3P_0	606	0.3
	2^3P_2	181	6.33		2^3P_2	185	6.71
	$2P'$	190	0.74		$2P'$	194	29
	$2P$	206	34		$2P$	210	0.24
	2^3P_0	232	0.04		2^3P_0	236	0.05

TABLE VII. Partial widths of the $E1$ dominant radiative transitions for the $2S$-, $2P$-wave B_c states. For comparison, the predictions from the relativistic quark model [10], relativized quark model [11], nonrelativistic constituent quark models [7,9] are listed in the table as well.

		E_γ (MeV)					Γ_{E1} (keV)				Γ_{EM} (keV)
Initial state	Final state	[7]	[10]	[11]	[9]	Ours	[7]	[10]	[11]	[9]	Ours
2^3S_1	1^3P_2	151	118	118	159	102	17.7	7.59	5.7	14.8	6.98
	$1P_1'$	161	130	136	173	115	0	0.74	0.7	1.0	1.56
	$1P_1$	167	146	144	185	133	14.5	7.65	4.7	12.8	4.62
	1^3P_0	196	181	179	219	174	7.8	5.53	2.9	7.7	3.48
2^1S_0	$1P_1'$	119	84	104	138	96	5.2	4.40	6.1	15.9	6.38
	$1P_1$	125	101	113	150	114	0	1.05	1.3	1.9	5.33
2^3P_2	1^3D_3	142	75	118	127	129	17.8	2.08	6.8	10.9	14
	$1D_2'$		77	122	118	127		0.139	0.6	0.5	0.93
	$1D_2$		79	127	133	135		0.285	0.7	1.5	1.1
	1^3D_1	142	84	135	126	139	0.2	0.035	0.1	0.1	0.13
	2^3S_1	249	270	272	232	265	73.8	75.3	55	49.4	50
	1^3S_1	770		778	817	785	25.8		14	25.8	52
$2P_1'$	$1D_2'$		66	113	108	117		1.49	5.5	3.5	1.05
	$1D_2$		68	123	123	125		0.172	1.3	2.5	0.03
	1^3D_1	131	73	121	116	129	0.4	0.07	0.2	0.3	1.27
	2^3S_1	239	259	258	222	255	5.4	10.4	5.5	5.9	25
	1^3S_1	760		769	807	777	2.1		0.6	2.5	26
	2^1S_0		303	289	257	274		90.5	52	58.0	36
	1^1S_0			825	871	825			19	131.1	44
$2P_1$	$1D_2'$		47	108	97	101		0.023	0.8	1.2	0.006
	$1D_2$		49	103	112	109		0.517	3.6	3.9	0.84
	1^3D_1	125	54	116	105	113	0.3	0.204	1.6	1.6	1.45
	2^3S_1	232	241	253	211	240	54.3	45.3	45	32.1	34
	1^3S_1	754		761	796	762	22.1		5.4	15.3	40
	2^1S_0		285	284	246	258		13.8	5.7	8.1	19
	1^1S_0			820	860	811			2.1	3.1	25
2^3P_0	1^3D_1	98	19	93	80	86	6.9	0.041	4.2	3.2	5.6
	2^3S_1	205	207	231	186	214	41.2	34	42	25.5	53
	1^3S_1	729		741	771	738	21.9		1	16.1	41

TABLE VIII. Partial widths of the $E1$ dominant radiative transitions for the $3S$-, $4S$-, $3P$-wave B_c states.

Initial state	Final state	E_γ (MeV)	$\Gamma_{\rm EM}$ (keV)	Initial state	Final state	E_γ (MeV)	$\Gamma_{\rm EM}$ (keV)
3^1S_0	$2P'$	88	11.13	3^3S_1	2^3P_2	91	11.89
	$2P$	104	10.93		$2P'$	101	2.92
	$1P'$	450	1.74		$2P$	117	7.2
	$1P$	467	1.25		2^3P_0	144	5
					1^3P_2	450	1.58
					$1P'$	462	0.7
					$1P$	479	1.72
					1^3P_0	518	1.73
4^1S_0	$1P'$	727	1.93	4^3S_1	1^3P_2	724	1.88
	$1P$	743	1.7		$1P'$	736	0.82
	$2P'$	380	6.31		$1P$	752	1.37
	$2P$	395	5.14		1^3P_0	790	1.3
	$3P'$	82	13		2^3P_2	380	5.78
	$3P$	98	17		$2P'$	389	1.96
					$2P$	405	4.04
					2^3P_0	430	3.28
					3^3P_2	86	16
					$3P'$	91	4.06
					$3P$	108	8.71
					3^3P_0	129	6.12
3^3P_0	2^3D_1	84	10.93	3^3P_2	2^3D_3	115	22
	1^3D_1	389	1.84		$2D'$	116	1.57
	3^3S_1	166	45		$2D$	120	1.72
	2^3S_1	511	36		2^3D_1	127	0.23
	1^3S_1	1013	30		1^3D_3	421	9.07
					$1D'$	419	1.06
					$1D$	427	1.16
					1^3D_1	431	0.94
					3^3S_1	209	43
					2^3S_1	552	39
					1^3S_1	1051	42
$3P_1$	$2D'$	93	0.003	$3P_1'$	$2D'$	110	1.9
	$2D$	97	1.3		$2D$	114	0.05
	2^3D_1	104	2.39		2^3D_1	121	2.47
	$1D'$	398	0.74		$1D'$	414	0.19
	$1D$	405	0.31		$1D$	421	0.93
	1^3D_1	409	0.67		1^3D_1	425	0.61
	3^3S_1	187	26		3^3S_1	203	25
	2^3S_1	531	27		2^3S_1	546	22
	1^3S_1	1031	30		1^3S_1	1046	24
	3^1S_0	199	18		3^1S_0	216	30
	2^1S_0	548	19		2^1S_0	564	28
	1^1S_0	1078	23		1^1S_0	1093	32

$\mathcal{Y}_{\ell m}(\mathbf{k}) \equiv |\mathbf{k}|^\ell Y_{\ell m}(\theta_\mathbf{k}, \phi_\mathbf{k})$ is the ℓ-th solid harmonic polynomial. The factor (-3) is introduced for convenience, which will cancel the color factor.

For an OZI-allowed two-body strong decay process $A \to B + C$, the helicity amplitude $\mathcal{M}^{M_{J_A} M_{J_B} M_{J_C}}(\mathbf{P})$ can be derived as follows:

$$\langle BC|T|A\rangle = \delta(\mathbf{P}_A - \mathbf{P}_B - \mathbf{P}_C)\mathcal{M}^{M_{J_A} M_{J_B} M_{J_C}}(\mathbf{P}). \tag{18}$$

Using the Jacob-Wick formula [79], one can convert the helicity amplitudes $\mathcal{M}^{M_{J_A} M_{J_B} M_{J_C}}(\mathbf{P})$ to the partial wave amplitudes $\mathcal{M}^{JL}$ via

$$\mathcal{M}^{JL}(A \to BC) = \frac{\sqrt{4\pi(2L+1)}}{2J_A+1} \sum_{M_{J_B}, M_{J_C}} \langle L0JM_{J_A}|J_A M_{J_A}\rangle \times \langle J_B M_{J_B} J_C M_{J_C}|JM_{J_A}\rangle \mathcal{M}^{M_{J_A} M_{J_B} M_{J_C}}(\mathbf{P}). \tag{19}$$

TABLE IX. The masses (MeV) of the final hadrons appearing in the strong decay processes of the B_c states. The masses are taken from the Particle Data Group [83] if there are experimental data; otherwise we take the quark model predictions in Refs. [81,82].

State	1^1S_0	1^3S_1	1^3P_0	$1P_1$	$1P_1'$	1^3P_2
B	5279	5325	5683	5729	5754	5768
B_s	5367	5415	5756	5801	5836	5851
D	1870	2010	2252	2402	2417	2466
D_s	1968	2112	2344	2488	2510	2559

In the above equations, (J_A, J_B and J_C), (L_A, L_B and L_C), and (S_A, S_B and S_C) are the quantum numbers of the total angular momenta, orbital angular momenta, and total spin for hadrons A, B, C, respectively; $M_{J_A} = M_{J_B} + M_{J_C}$, $\mathbf{J} \equiv \mathbf{J}_B + \mathbf{J}_C$, and $\mathbf{J}_A \equiv \mathbf{J}_B + \mathbf{J}_C + \mathbf{L}$. In the c.m. frame of hadron A, the momenta $\mathbf{P}_B$ and $\mathbf{P}_C$ of mesons B and C satisfy $\mathbf{P}_B = -\mathbf{P}_C \equiv \mathbf{P}$.

Then the strong decay partial width for a given decay mode of $A \to B + C$ is given by

$$\Gamma = 2\pi|\mathbf{P}|\frac{E_B E_C}{M_A}\sum_{JL}|\mathcal{M}^{JL}|^2, \tag{20}$$

where M_A is the mass of the initial hadron A, while E_B and E_C stand for the energies of final hadrons B and C, respectively. The details of the $^3P_0$ model can be found in our recent paper [80].

In the calculations, the wave functions of the initial B_c states are adopted from our quark model predictions. Furthermore, we need the wave functions of the final hadrons, i.e., the $B^{(*)}$, $B_s^{(*)}$, $D^{(*)}$, $D_s^{(*)}$ mesons and some of their excitations, which are adopted from the quark model predictions of Refs. [81,82].

In this work, for the masses of the light constituent u, d, and s quarks, we set $m_u = m_d = 0.33$ GeV, $m_s = 0.45$ GeV; while for the heavy b and c quarks, their masses are taken to be $m_b = 4.852$ GeV and $m_c = 1.483$ GeV as the determinations in the calculations of the B_c mass spectrum. The masses of the final hadron states in the decay processes are adopted from the Particle Data Group [83] if there are measured values; otherwise we take the quark model predictions of Refs. [81,82] (see Table IX). There is no experimental data which can be used to determine the quark pair creation strength; thus, in this work we adopt a typical value $\gamma = 0.4$ that gives a reasonably accurate description of the overall scale of decay widths of both light and heavy mesons [66,84–88]. The strong decay properties for the bottom-charmed states are presented in Table X–XV.

V. DISCUSSION

A. S-wave states

Recently, signals of two excited $\bar{b}c$ states, $B_c(2S)$ and $B_c^*(2S)$, were observed in the $B_c^+\pi^+\pi^-$ invariant mass spectrum by the CMS Collaboration at LHC. These two states are well resolved from each other and are observed with a significance exceeding five standard deviations. The mass of $B_c(2S)$ meson is measured to be 6871 ± 2.8 MeV. Furthermore, a more precise mass of $B_c(2S)$, $M(B_c^+) = 6871.1 \pm 0.5$ MeV, is measured by the CMS Collaboration as well. Combining these newest measurements, we predict that the mass of $B_c(2S)$ might be ~6890 MeV, and the mass hyperfine splitting between $B_c^*(2S)$ and $B_c(2S)$,

$$\Delta m(2S) \simeq 20 \text{ MeV}, \tag{21}$$

is slightly smaller than 30–45 MeV, predicted in previous works (see Table I). The predicted masses for the other higher S-wave states compared with other works are also given in Table I. Obvious differences can be found in various theoretical predictions.

The $M1$ transitions of the low-lying S-wave states $B_c^*(2S)$ and $B_c^{(*)}(1S)$ were often discussed in the literature for these transitions which might be used to establish them in experiments. In this work we also calculate their $M1$ transitions. Our results compared with some other predictions are listed Table III. Obvious model dependence can be seen in various calculations. Our predicted partial width,

$$\Gamma[B_c^*(2S) \to B_c\gamma] \simeq 1.2 \text{ keV}, \tag{22}$$

for the $M1$ transition $B_c^*(2S) \to B_c\gamma$ is about an order of magnitude larger than that predicted in Refs. [7,9,10], and about a factor 2 larger than the value predicted within the GI model [11]. Combining our calculations of the EM transitions $B_c^*(2S) \to 1P\gamma$ and the strong transitions $B_c^*(2S) \to B_c^*\pi\pi$ predicted in [11], the total decay width of $B_c^*(2S)$ meson is estimated to be $\Gamma_{\text{total}} \sim 75$ keV; then the branching fraction for $M1$ transition $B_c^*(2S) \to B_c\gamma$ is predicted to be

$$\text{Br}[B_c^*(2S) \to B_c\gamma] \sim 2\%. \tag{23}$$

The fairly large branching fraction may give a good opportunity for us to observe the $B_c^*(2S)$ via the $M1$ transition $B_c^*(2S) \to B_c\gamma$. This process may be used to determined the mass of $B_c^*(2S)$ in future experiments.

The masses of $3S$-wave states $B_c(3^1S_0)$ and $B_c(3^3S_1)$ are predicted to be ~7.24 GeV and ~7.25 GeV, respectively, which are just above the DB^* threshold. Their radiative and strong decay properties are estimated in this work. The results for the $M1$ transitions, $E1$ dominant transitions, and strong decays of the $3S$-wave states are given in Tables III, VI, and X, respectively. There are only a few works about the radiative and strong decay properties of the $3S$-wave states [11,18,59,60]. The $M1$ transitions of the $3S$-wave states roughly agree with the predictions in Ref. [11], except that our predicted partial width $\Gamma[3^3S_1 \to 1^1S_0 + \gamma] \simeq 510$ eV for the $M1$ transition

TABLE X. Strong decay properties for the $4S$-, $5S$-wave B_c states. Γth and B_r stand for the partial widths and branching ratios of the strong decay processes, respectively.

State	Decay mode	Γ_{th} (MeV)	$B_r(\%)$	State	Decay mode	Γ_{th} (MeV)	$B_r(\%)$
$3^1S_0(7239)$	B^*D	161	100	$3^3S_1(7252)$	BD	28	21
					B^*D	105	79
	Total	161	100		Total	133	100
$4^1S_0(7540)$	B^*D	0.14	0.1	$4^3S_1(7550)$	BD	4.53	2.7
	BD^*	34.9	18.3		B^*D	0.41	0.2
	B^*D^*	104	54		BD^*	17.0	10
	$B_s^{*0}D_s^+$	6.7	3.5		B^*D^*	112	66
	$B_s^0D_s^{*+}$	5.8	3.1		$B_s^0D_s^+$	2.81	1.6
	$B_s^{*0}D_s^{*+}$	15.5	8.1		$B_s^{*0}D_s^+$	5.29	3.1
	$BD(1^3P_0)$	24	12.6		$B_s^0D_s^{*+}$	1.83	1.1
					$B_s^{*0}D_s^{*+}$	26.9	16
	Total	191	100		Total	171	100
$5^1S_0(7805)$	B^*D	24.5	5.9	$5^3S_1(7813)$	BD	15.81	3.9
	BD^*	1.5	0.4		B^*D	20.18	5
	B^*D^*	2.28	0.6		BD^*	2.65	0.7
	$B_s^{*0}D_s^+$	1.62	0.4		B^*D^*	0.19	0.05
	$B_s^0D_s^{*+}$	4.65	1.1		$B_s^0D_s^+$	0.02	0.005
	$B_s^{*0}D_s^{*+}$	5.75	1.4		$B_s^{*0}D_s^+$	0.62	0.2
	$B(1^3P_0)D$	18.6	4.5		$B_s^0D_s^{*+}$	3.02	0.8
	$B(1^3P_2)D$	27.6	6.7		$B_s^{*0}D_s^{*+}$	8.09	2
	$B(1P')D^*$	82	19.9		$B(1P')D$	18.96	4.7
	$B(1P)D^*$	6.2	1.5		$B(1P)D$	13.34	3.3
	$B(1^3P_2)D^*$	56.5	13.7		$B(1^3P_2)D$	16.1	4
	$BD(1^3P_0)$	23.5	5.7		$B(1^3P_0)D^*$	0.04	0.01
	$BD(1^3P_2)$	48.2	11.7		$B(1P')D^*$	53.93	13.4
	$B^*D(1P')$	70.9	17.2		$B(1P)D^*$	5.19	1.3
	$B^*D(1P)$	12.3	3.0		$B(1^3P_2)D^*$	96	24
	$B^*D(1^3P_2)$	25.7	6.2		$BD(1P')$	0.89	0.2
	$B_S(1^3P_0)D_S$	0.17	0.04		$BD(1P)$	0.63	0.2
	$B_SD_S(1^3P_0)$	0.56	0.14		$BD(1^3P_2)$	17.34	4.3
					$B^*D(1^3P_0)$	18.32	4.6
					$B^*D(1P')$	32.9	8.2
					$B^*D(1P)$	6.8	1.7
					$B^*D(1^3P_2)$	69.87	17
					$B_S(1P')D_S$	0.36	0.09
					$B_S(1P)D_S$	0.01	0.002
					$B_S^*D_S(1^3P_0)$	0.3	0.07
	Total	413	100		Total	401	100

$3^3S_1 \to 1^1S_0 + \gamma$ is about an order of magnitude smaller than that in Ref. [11]. The strong decay widths of $B_c(3^1S_0)$ and $B_c(3^3S_1)$ predicted by us are comparable with those predicted in recent works [18,59]. Both $B_c(3^1S_0)$ and $B_c(3^3S_1)$ might be broad states with a width of ~100 MeV. The $B_c(3^1S_0)$ dominantly decay into DB^* channel, while $B_c(3^3S_1)$ dominantly decay into both DB and DB^* channels. The production rates of the $3S$-wave B_c states in pp collisions at the LHC may be comparable with those of the $2S$-wave B_c states [18]; thus, the $3S$-wave B_c states may have large potentials to be established in the DB^* final states.

The higher S-wave states $B_c(n^1S_0)$ and $B_c(n^3S_1)$ ($n \geq 4$) are far from the DB threshold, thus many OZI-allowed two-body strong decay channels are open. There are few discussions of the decay properties of the higher mass S-wave states in the literature. To know some decay properties of these higher S-wave states, in this work we give our predictions of the $M1$ transitions and strong decays of $B_c(nS)$ ($n = 4, 5, 6$), which are listed in Tables IV and X, respectively. It is found that these higher mass S-wave states are broad states with a width of ~100–400 MeV. Combining $M1$ transitions of higher S-wave states with their strong decays, we find that the branching fractions of

TABLE XI. Strong decay properties for the 6S-wave B_c states.

State	Decay mode	Γ_{th} (MeV)	$B_r(\%)$	State	Decay mode	Γ_{th} (MeV)	$B_r(\%)$
$6^1S_0(8046)$	B^*D	44.4	12	$6^3S_1(8054)$	BD	17.6	4.7
	BD^*	24.3	6.7		B^*D	31	8.3
	B^*D^*	24.3	6.7		BD^*	19.1	5.1
	$B_s^{*0}D_s^+$	1.11	0.3		B^*D^*	37.9	10.2
	$B_s^0D_s^{*+}$	0.38	0.11		$B_s^0D_s^+$	1.78	0.5
	$B_s^{*0}D_s^{*+}$	3.33	0.9		$B_s^{*0}D_s^+$	1.22	0.3
	$B(1^3P_0)D$	11.3	3.1		$B_s^0D_s^{*+}$	0.09	0.02
	$B(1^3P_2)D$	4.85	1.3		$B_s^{*0}D_s^{*+}$	2.96	0.8
	$B(1P')D^*$	28.3	7.8		$B(1P')D$	0.25	0.07
	$B(1P)D^*$	24.7	6.8		$B(1P)D$	11.1	3
	$B(1^3P_2)D^*$	20.6	5.7		$B(1^3P_2)D$	1.09	0.3
	$BD(1^3P_0)$	13.2	3.6		$B(1^3P_0)D^*$	10.9	3
	$BD(1^3P_2)$	28.9	8		$B(1P')D^*$	21.2	5.7
	$B^*D(1P')$	46.8	13		$B(1P)D^*$	17	4.6
	$B^*D(1P)$	41.4	11.4		$B(1^3P_2)D^*$	34	9.1
	$B^*D(1^3P_2)$	23.5	6.5		$BD(1P')$	9.37	2.5
	$B_s(1^3P_0)D_s$	5.5	1.5		$BD(1P)$	16.6	4.4
	$B_s(1^3P_2)D_s$	0.17	0.05		$BD(1^3P_2)$	14.1	3.8
	$B_s(1P')D_s^*$	0.88	0.24		$B^*D(1^3P_0)$	12.9	3.5
	$B_s(1P)D_s^*$	0.03	0.01		$B^*D(1P')$	30.5	8.2
	$B_s(1^3P_2)D_s^*$	0.02	0.01		$B^*D(1P)$	27.9	7.5
	$B_sD_s(1^3P_0)$	6.62	1.8		$B^*D(1^3P_2)$	39.9	10.7
	$B_sD_s(1^3P_2)$	2.47	0.68		$B_s(1P')D_s$	0.61	0.2
	$B_s^*D_s(1P')$	4.14	1.1		$B_s(1P)D_s$	3.06	0.8
	$B_s^*D_s(1P)$	0.23	0.06		$B_s(1^3P_2)D_s$	0.24	0.1
	$B_s^*D_s(1^3P_2)$	0.18	0.05		$B_s(1^3P_0)D_s^*$	0.001	0.0003
					$B_s(1P')D_s^*$	1.13	0.3
					$B_s(1P)D_s^*$	0.005	0.001
					$B_s(1^3P_2)D_s^*$	0.48	0.1
					$B_sD_s(1P')$	0.56	0.2
					$B_sD_s(1P)$	0.04	0.01
					$B_sD_s(1^3P_2)$	1.35	0.4
					$B_s^*D_s(1^3P_0)$	3.3	0.9
					$B_s^*D_s(1P')$	3.06	0.8
					$B_s^*D_s(1P)$	0.21	0.1
					$B_s^*D_s(1^3P_2)$	0.03	0.008
	Total	361	100		Total	372	100

the $M1$ transitions $B_c(nS) \to B_c(1S) + \gamma$ may reach up to a sizeable value $\mathcal{O}(10^{-5})$.

B. *P*-wave states

The masses of $1P$-wave states $B_c(1P)$ might lie in the range of (6710,6790) MeV, which are consistent with the other predictions with potential models [7–11], and the recent lattice calculations [36]. The $1P$-wave $B_c(1P)$ states mainly decay via the $E1$ dominate transitions $1P \to 1S$. We have calculated the partial decay widths for the EM transitions $1P \to 1S$; our results compared with some other predictions are listed in Table V. Most of our results are compatible with the predictions in [7,9–11], except our predicted partial decay widths of $\Gamma[B_c(1P_1) \to B_c\gamma] \simeq 35$ keV and $\Gamma[B_c(1P_1') \to B_c^*\gamma] \simeq 40$ keV are about a factor of 3–5 larger than the predictions in Refs. [9–11]. The $B_c(1P_1)$ and $B_c(1P_1')$ states might be first found in the $B_c\gamma$ final state via their radiative transitions. The branching fractions for $B_c(1P_1)$ and $B_c(1P_1')$ decay into $B_c\gamma$ are predicted to be

$$Br[B_c(1P_1) \to B_c\gamma] \sim 33\%, \tag{24}$$

$$Br[B_c(1P_1') \to B_c\gamma] \sim 65\%. \tag{25}$$

While the $B_c(1^3P_0)$ and $B_c(1^3P_2)$ states dominantly decay into the $B_c^*\gamma$ final state with a decay rate of $\sim$100%, they

TABLE XII. Strong decay properties for the $3P$-, $4P$-wave B_c states.

State	Decay mode	Γ_{th} (MeV)	$B_r(\%)$	State	Decay mode	Γ_{th} (MeV)	$B_r(\%)$
$3^3P_0(7420)$	BD	9.6	3.5	$3^3P_2(7464)$	BD	22	11.1
	B^*D^*	255	93		B^*D	16	8.1
	$B_s^0D_s^+$	9.7	3.5		BD^*	3.4	1.7
					B^*D^*	146	74
					$B_s^0D_s^+$	2.7	1.4
					$B_s^{*0}D_s^+$	7.8	4
	Total	274	100		Total	198	100
$3P_1'(7458)$	B^*D	13.6	7.3	$3P_1(7441)$	B^*D	9.3	4.3
	BD^*	32	17.2		BD^*	62	28.1
	B^*D^*	129	69.4		B^*D^*	145	65.8
	$B_s^{*0}D_s^+$	11.1	6		$B_s^{*0}D_s^+$	4.0	1.8
	Total	185	100		Total	220	100
$4^3P_0(7693)$	BD	13.6	25.6	$4^3P_2(7732)$	BD	21.76	11.4
	B^*D^*	14	26.4		B^*D	30.1	15.8
	$B_s^0D_s^+$	7.16	13.5		BD^*	13.9	7.3
	$B_s^{*0}D_s^{*+}$	4.6	8.7		B^*D^*	7.82	4.1
	$B(1P')D$	7.66	14.4		$B_s^0D_s^+$	0.84	0.4
	$B(1P)D$	0.44	0.83		$B_s^{*0}D_s^+$	0.01	0.005
	$BD(1P)$	0.07	0.13		$B_s^0D_s^{*+}$	2.34	1.2
	$B^*D(1^3P_0)$	5.5	10.4		$B_s^{*0}D_s^{*+}$	11.1	5.8
					$B(1P')D$	27.7	14.5
					$B(1P)D$	6.95	3.6
					$B(1^3P_2)D$	20.2	10.6
					$B(1^3P_0)D^*$	8.8	4.6
					$BD(1P')$	13.1	6.9
					$BD(1P)$	6.61	3.5
					$B^*D(1^3P_0)$	10.1	5.3
					$B^*D(1P)$	9.22	4.8
	Total	53	100		Total	190	100
$4P_1'(7727)$	B^*D	41.6	29.1	$4P_1(7710)$	B^*D	24.5	19.4
	BD^*	11.9	8.4		BD^*	3.7	2.9
	B^*D^*	6.55	4.6		B^*D^*	0.86	0.7
	$B_s^{*0}D_s^+$	1.42	1.0		$B_s^{*0}D_s^+$	4.4	3.5
	$B_s^0D_s^{*+}$	6.2	4.3		$B_s^0D_s^{*+}$	6.78	5.4
	$B_s^{*0}D_s^{*+}$	9.09	6.3		$B_s^{*0}D_s^{*+}$	6.66	5.3
	$B(1^3P_0)D$	10.4	7.3		$B(1^3P_0)D$	0.002	0.002
	$B(1P')D$	0.003	0.002		$B(1P')D$	0.4	0.3
	$B(1P)D$	0.01	0.01		$B(1P)D$	3.32	2.6
	$B(1^3P_2)D$	36.6	25.6		$B(1^3P_2)D$	15	11.9
	$B(1^3P_0)D^*$	0.02	0.01		$B(1^3P_0)D^*$	11.8	9.4
	$BD(1^3P_0)$	13.6	9.5		$BD(1^3P_0)$	0.1	0.08
	$BD(1P')$	0.009	0.006		$BD(1P')$	15.32	12.2
	$BD(1P)$	0.05	0.03		$BD(1P)$	23.03	18.3
	$B^*D(1^3P_0)$	0.1	0.07		$B^*D(1^3P_0)$	10.02	8.0
	$B^*D(1P)$	0.31	0.22				
	$B_sD_s(1^3P_0)$	4.75	3.3				
	$B_s(1^3P_0)D_s$	0.41	0.3				
	Total	143	100		Total	126	100

have good potential to be found via the radiative decay chains $B_c(1^3P_0)\to B_c(1^3S_1)\gamma\to B_c(1^1S_0)\gamma\gamma$ and $B_c(1^3P_2)\to B_c(1^3S_1)\gamma\to B_c(1^1S_0)\gamma\gamma$, respectively.

For the $2P$-wave states $B_c(2P)$, their masses might lie in the range (7100,7160) MeV, which are consistent with the other model predictions in the literature [7–11,15,16]. The masses for $B_c(2^3P_0)$ and $B_c(2P_1)$ are slightly lower than the DB mass threshold, while $B_c(2P_1')$ and $B_c(2^3P_2)$ slightly lie above the DB mass threshold. The $B_c(2^3P_2)$ state mainly decays into the DB channel, while its radiative

TABLE XIII. Strong decay properties for the $2D$-, $3D$-wave B_c states.

State	Decay mode	$\Gamma_{\rm th}$ (MeV)	$B_r(\%)$	State	Decay mode	Γ_{th} (MeV)	$B_r(\%)$
$2^3D_1(7336)$	BD	0.55	1.0	$2^3D_3(7348)$	BD	41.6	22.1
	B^*D	6.24	10.9		B^*D	50.8	26.9
	BD^*	50.1	87		BD^*	9.29	4.9
	B^*D^*	0.48	0.8		B^*D^*	87	46.1
	$B_s^0D_s^+$	0.18	0.3		$B_s^0D_s^+$	0.013	0.01
	Total	57	100		Total	189	100
$2D_2'(7347)$	B^*D	57.1	34.7	$2D_2(7343)$	B^*D	38.2	27
	BD^*	66.8	40.7		BD^*	89	64
	B^*D^*	40.4	24.6		B^*D^*	12.3	9
	Total	164	100		Total	139	100
$3^3D_1(7611)$	BD	25.2	28.2	$3^3D_3(7625)$	BD	19.3	17
	B^*D	5.65	6.3		B^*D	29.7	26.5
	BD^*	0.48	0.5		BD^*	20.8	18.6
	B^*D^*	19.5	21.9		B^*D^*	18.4	16.4
	$B_s^0D_s^+$	2.27	2.5		$B_s^0D_s^+$	1.45	1.3
	$B_s^{*0}D_s^+$	3.16	3.5		$B_s^{*0}D_s^+$	0.12	0.1
	$B_s^0D_s^{*+}$	1.82	2.0		$B_s^0D_s^{*+}$	2.94	2.6
	$B_s^{*0}D_s^{*+}$	16.5	18.5		$B_s^{*0}D_s^{*+}$	6.6	5.9
	$B(1P)D$	0.76	0.9		$B(1P')D$	0.001	0.001
	$B^*D(1^3P_0)$	13.9	15.6		$B(1P)D$	4.62	4.1
					$B^*D(1^3P_0)$	8.14	7.3
	Total	89	100		Total	112	100
$3D_2'(7623)$	B^*D	45.8	34.6	$3D_2(7620)$	B^*D	38.9	34.2
	BD^*	20.6	15.6		BD^*	13.8	12
	B^*D^*	21.1	16		B^*D^*	22.1	19
	$B_s^{*0}D_s^+$	2.25	1.7		$B_s^{*0}D_s^+$	3.89	3.4
	$B_s^0D_s^{*+}$	6.33	4.8		$B_s^0D_s^{*+}$	6.46	5.7
	$B_s^{*0}D_s^{*+}$	9.07	6.8		$B_s^{*0}D_s^{*+}$	11.6	10
	$B(1^3P_0)D$	12.1	9.1		$B(1^3P_0)D$	0.03	0.03
	$B(1P)D$	0.02	0.02		$B(1P)D$	2.82	2.5
	$BD(1^3P_0)$	14.4	10.9		$BD(1^3P_0)$	0.65	0.6
	$B^*D(1^3P_0)$	0.65	0.5		$B^*D(1^3P_0)$	13.6	12
	Total	132	100		Total	114	100

decay rates into the $B_c(n^3S_1)\gamma$ ($n = 1, 2$) are also sizeable. Their partial widths are predicted to be

$$\Gamma[B_c(2^3P_2) \to DB] \simeq 760 \text{ keV}, \tag{26}$$

$$\Gamma[B_c(2^3P_2) \to B_c^*\gamma] \simeq 52 \text{ keV}, \tag{27}$$

$$\Gamma[B_c(2^3P_2) \to B_c^*(2S)\gamma] \simeq 50 \text{ keV}. \tag{28}$$

Thus, the total width of $B_c(2^3P_2)$ is $\Gamma_{\rm total}[B_c(2^3P_2)] \simeq 880$ keV. The $B_c(2^3P_2)$ state may have potential to be observed in the DB and $B_c\gamma$ final states, while for the $B_c(2^3P_0)$, $B_c(2P_1)$, and $B_c(2P_1')$ states, their decays are governed by the EM transitions. The radiative decay properties of these states have been given in Table VII. With these predictions, the total widths for $B_c(2^3P_0)$, $B_c(2P_1)$, and $B_c(2P_1')$ are estimated to be $\Gamma_{\rm total}[B_c(2^3P_0)] \simeq 100$ keV, $\Gamma_{\rm total}[B_c(2P_1)] \simeq 120$ keV, and $\Gamma_{\rm total}[B_c(2P_1')] \simeq 133$ keV, respectively. The branching fractions for $B_c(2P_1) \to B_c\gamma$, $B_c(2P_1') \to B_c\gamma$ and $B_c(2^3P_0) \to B_c^*\gamma$ are predicted to be

$$Br[B_c(2P_1) \to B_c\gamma] \simeq 20\%, \tag{29}$$

$$Br[B_c(2P_1') \to B_c\gamma] \simeq 33\% \tag{30}$$

$$Br[B_c(2^3P_0) \to B_c^*\gamma] \simeq 41\%. \tag{31}$$

The large branching fractions indicate that $B_c(2P_1)$ and $B_c(2P_1')$ may be established in the $B_c\gamma$ channel, while $B_c(2^3P_0)$ may be observed via the radiative decay chain $B_c(2^3P_0) \to B_c^*\gamma \to B_c\gamma\gamma$. It should be pointed out that the $B_c(2P_1)$, $B_c(2P_1')$, and $B_c(2^3P_2)$ states may lie above the B^*D threshold, so they may have fairly large strong decay

TABLE XIV. Strong decay properties for the $1F$-, $2F$-wave B_c states.

State	Decay mode	Γ_{th} (MeV)	$B_r(\%)$	State	Decay mode	Γ_{th} (MeV)	$B_r(\%)$
$1^3F_2(7235)$	BD	61.9	85	$1^3F_4(7227)$	BD	0.85	97
	B^*D	11.1	15		B^*D	0.03	3
	Total	73	100		Total	0.88	100
$1F'_3(7240)$	B^*D	15.1	100	$1F_3(7224)$	B^*D	8.53	100
	Total	15.1	100		Total	8.53	100
$2^3F_2(7518)$	BD	45.1	20.2	$2^3F_4(7514)$	BD	8	6
	B^*D	19.2	8.6		B^*D	20.9	16
	BD^*	0.39	0.2		BD^*	37.7	29
	B^*D^*	151	68		B^*D^*	57	43
	$B_s^0D_s^+$	0.68	0.3		$B_s^0D_s^+$	4.48	3.4
	$B_s^{*0}D_s^+$	3.63	1.6		$B_s^{*0}D_s^+$	3.26	2.5
	$B_s^0D_s^{*+}$	3.17	1.4		$B_s^0D_s^{*+}$	0.05	0.04
	Total	223	100		Total	131	100
$2F'_3(7525)$	B^*D	45.2	25	$2F_3(7508)$	B^*D	43.9	25
	BD^*	41.0	23		BD^*	30.2	17
	B^*D^*	80.3	45		B^*D^*	90.2	52
	$B_s^{*0}D_s^+$	7.19	4		$B_s^{*0}D_s^+$	7.78	4.5
	$B_s^0D_s^{*+}$	4.53	3		$B_s^0D_s^{*+}$	2.57	1.5
	Total	178	100		Total	175	100

widths $\mathcal{O}(10–100)$ MeV into B^*D and/or BD channels as predicted in Ref. [17].

For the higher P-wave states $B_c(nP)$ ($n = 3$, 4), many OZI-allowed strong decay channels are open (see Table XII); thus, these states usually are broad states with a width of $\mathcal{O}(100)$ MeV, except the $B_c(4^3P_0)$ state which has a relatively narrow width of $\mathcal{O}(10)$ MeV. The $B_c(4^3P_0)$ state may be first observed in the DB channel; the branching fraction for the process $B_c(4^3P_0) \to DB$ can reach up to ∼20%.

C. D-wave states

The masses of the $1D$-wave states $B_c(1D)$ are predicted to be ∼7.02 GeV in this work. The mass splitting between the $1D$-wave states is no more than 15 MeV. The masses predicted by us are consistent with the results in Refs. [7,8,11]. The $1D$-wave states mainly decay via the EM transitions, which have been given in Table V. It is seen that our main results are in reasonable agreement with the other predictions. Our study indicates that the $B_c(1^3D_3)$ state may have a relatively large potential to be observed via the radiative decay chain $B_c(1^3D_3) \to B_c(1^3P_2)\gamma \to B_c(1^3S_1)\gamma\gamma \to B_c(1^1S_0)\gamma\gamma\gamma$, and the branching fraction for this chain is estimated to be ∼100%. The optimal decay chain for the observations of $B_c(1^3D_1)$ is $B_c(1^3D_1) \to B_c(1^3P_0)\gamma \to B_c(1^3S_1)\gamma\gamma \to B_c(1^1S_0)\gamma\gamma\gamma$, and the branching fraction for this chain is estimated to be ∼60%. The optimal decay chains for the observations of $B_c(1D_2)$ are $B_c(1D_2) \to B_c(1P_1)\gamma \to B_c(1^3S_1)\gamma\gamma \to B_c(1^1S_0)\gamma\gamma\gamma$ and $B_c(1D_2) \to B_c(1P_1)\gamma \to B_c(1^1S_0)\gamma\gamma$, and the branching fractions for these chains are estimated to be ∼50% and ∼30%, respectively. For the observations of $B_c(1D'_2)$, the optimal decay chains are $B_c(1D'_2) \to B_c(1P'_1)\gamma \to B_c(1^3S_1)\gamma\gamma \to B_c(1^1S_0)\gamma\gamma\gamma$ and $B_c(1D'_2) \to B_c(1P'_1)\gamma \to B_c(1^1S_0)\gamma\gamma$, and the branching fractions for these chains are estimated to be ∼35% and ∼47%, respectively.

The masses of the $2D$ states are predicted to be ∼7.34 GeV, which is very close to the D_sB_s threshold. Their decays are governed by the strong decay modes, such as DB, DB^*, BD^*, or B^*D^*. Their strong decay properties predicted by us have been listed in Table XIII. There are few discussions about the radiative decays of the $2D$-wave B_c states in the literature. In this work, we also calculate their radiative decay properties; our results are given in Table VI. It is found that the $B_c(2^3D_1)$ state has a relatively narrow width of $\Gamma \sim 58$ MeV. The decays of $B_c(2^3D_1)$ are governed by the BD^* mode with a branching fraction

$$\mathrm{Br}[B_c(2^3D_1) \to BD^*] \simeq 87\%. \tag{32}$$

The other three $2D$ states $B_c(2^3D_3)$, $B_c(2D_2)$, and $B_c(2D'_2)$ are broad states with a width of ∼100–200 MeV. The $B_c(2^3D_3)$ state mainly decays into DB, DB^*, and B^*D^* channels. While the $B_c(2D_2)$ and $B_c(2D'_2)$ states dominantly decay into DB^*, BD^*, or B^*D^* channels. Combing the strong and radiative decay properties with each other, it is found that the branching fractions of the dominant EM decay processes $B_c(2D) \to B_c(nP)$ ($n = 1$, 2) are $\mathcal{O}(10^{-4})$. The observations of the DB, DB^*, BD^*, or B^*D^* final states might be useful to search for these missing $2D$ states in future experiments.

TABLE XV. Strong decay properties for the $3F$-wave B_c states.

State	Decay mode	Γ_{th} (MeV)	$B_r(\%)$	State	Decay mode	Γ_{th} (MeV)	$B_r(\%)$
$3^3F_2(7730)$	BD	32.1	14	$3^3F_4(7771)$	BD	2.82	1.6
	B^*D	16.1	7		B^*D	8.9	5.0
	BD^*	3.89	1.7		BD^*	20.2	11.4
	B^*D^*	72	31.5		B^*D^*	50.9	28.7
	$B_s^0D_s^+$	0.38	0.2		$B_s^0D_s^+$	3.2	1.8
	$B_s^{*0}D_s^+$	0.11	0.05		$B_s^{*0}D_s^+$	3.2	1.8
	$B_s^0D_s^{*+}$	2.09	0.9		$B_s^0D_s^{*+}$	0.4	0.2
	$B_s^{*0}D_s^{*+}$	5.25	2.3		$B_s^{*0}D_s^{*+}$	9.19	5.2
	$B(1P')D$	19.5	8.5		$B(1P')D$	19.4	10.9
	$B(1P)D$	5.03	2.2		$B(1P)D$	1.85	1.04
	$B(1^3P_2)D$	12.1	5.3		$B(1^3P_2)D$	12.3	6.9
	$B(1^3P_0)D^*$	2.56	1.1		$B(1^3P_0)D^*$	6.82	3.8
	$BD(1P')$	45.8	20		$B(1P')D^*$	0.02	0.01
	$BD(1P)$	2.3	1		$B(1P)D^*$	3.03	1.7
	$B^*D(1^3P_0)$	9.14	4		$BD(1P')$	9.19	5.2
	$B^*D(1P)$	0.48	0.2		$BD(1P)$	11.2	6.3
					$BD(1^3P_2)$	1.61	0.9
					$B^*D(1^3P_0)$	1.91	1.1
					$B^*D(1P')$	2.83	1.6
					$B^*D(1P)$	8.42	4.7
					$B_s(1P)D_s$	<0.0001	≃0
					$B_s^*D_s(1^3P_0)$	0.02	0.01
	Total	228	100		Total	177	100
$3F_3'(7779)$	B^*D	33.6	11	$3F_3(7768)$	B^*D	39.9	12
	BD^*	34.4	11.3		BD^*	31.3	9.5
	B^*D^*	59.9	19.6		B^*D^*	63.5	19.3
	$B_s^{*0}D_s^+$	4.2	1.4		$B_s^{*0}D_s^+$	2.64	0.8
	$B_s^0D_s^{*+}$	1.69	0.6		$B_s^0D_s^{*+}$	2.02	0.6
	$B_s^{*0}D_s^{*+}$	4.85	1.6		$B_s^{*0}D_s^{*+}$	3.63	1.1
	$B(1^3P_0)D$	0.008	0.003		$B(1^3P_0)D$	0.01	0.003
	$B(1P')D$	0.01	0.003		$B(1P')D$	6.25	1.9
	$B(1P)D$	<0.001	≃0		$B(1P)D$	2.26	0.7
	$B(1^3P_2)D$	36.7	12		$B(1^3P_2)D$	27.6	8.4
	$B(1^3P_0)D^*$	0.08	0.03		$B(1^3P_0)D^*$	8.06	2.5
	$B(1P')D^*$	30.4	10		$B(1P')D^*$	8.69	2.6
	$B(1P)D^*$	7.75	2.5		$B(1P)D^*$	2.3	0.7
	$B(1^3P_2)D^*$	0.68	0.2		$BD(1^3P_0)$	0.6	0.2
	$BD(1^3P_0)$	0.11	0.04		$BD(1P')$	11.6	3.5
	$BD(1P')$	0.07	0.02		$BD(1P)$	16.6	5.1
	$BD(1P)$	0.56	0.2		$BD(1^3P_2)$	34.2	10
	$BD(1^3P_2)$	27.1	8.9		$B^*D(1^3P_0)$	1.73	0.53
	$B^*D(1^3P_0)$	0.13	0.04		$B^*D(1P')$	57.4	17.5
	$B^*D(1P')$	38.9	12.8		$B^*D(1P)$	8.23	2.5
	$B^*D(1P)$	19.2	6.3		$B_s(1^3P_0)D_s$	0.003	≃0
	$B_s(1^3P_0)D_s$	1.38	0.45		$B_sD_s(1^3P_0)$	0.14	0.04
	$B_s(1P)D_s$	<0.0001	≃0		$B_s^*D_s(1^3P_0)$	0.01	0.003
	$B_sD_s(1^3P_0)$	3.03	1.0				
	$B_s^*D_s(1^3P_0)$	0.01	0.003				
	Total	305	100		Total	329	100

The higher $3D$-wave states $B_c(3D)$ are also studied in the present work. The masses predicted by us are about 7.62 GeV, which are comparable with those predicted in Ref. [8], while they are about 150 MeV smaller than those predicted in Refs. [15,16]. The strong decay properties are shown in Table XIII. It is found that these higher $3D$-wave states have a width of ∼100 MeV. These higher states might be observed in their dominant strong decay channels.

D. *F*-wave states

The masses of the $1F$-wave states $B_c(1^3F_4)$, $B_c(1F_3)$, $B_c(1F'_3)$, and $B_c(1^3F_2)$ are predicted to be $\sim$7.23 GeV, which are comparable to those predicted in Refs. [8,11,16]. These $1F$ wave states lie above the mass threshold of DB and B^*D, while below the D^*B threshold. From our predictions of the strong decay properties for these $1F$ wave states (see Table XIV), it is found that the $B_c(1^3F_4)$ state might be a very narrow state with a width of $\sim$1 MeV, its decays are governed by the DB mode. Both $B_c(1F_3)$ and $B_c(1F'_3)$ are narrow states with a width of $\sim$10 MeV, they dominantly decay into the DB^* channel. The $B_c(1^3F_2)$ should be a relatively broad state with a width of $\sim$70 MeV; it mainly decays into the DB channel with a branching fraction of $\mathrm{Br}[B_c(1^3F_2) \to DB] \simeq 85\%$. To look for the missing $1F$-wave B_c states, the DB and B^*D final states are worth observing.

The predicted masses for the $2F$- and $3F$-wave B_c states are $\sim$7.5 GeV and $\sim$7.8 GeV, respectively, which are comparable with the predictions in Refs. [8,11]. There are many strong decay channels for these higher mass F-wave states. Our predictions of their strong decay properties have been listed in Tables XIV and XV. It is found that the higher mass F-wave states might be broad states with a width of $\sim$100–300 MeV.

VI. SUMMARY

In this paper, we have calculated the B_c meson spectrum up to the $6S$ states with a nonrelativistic linear potential model by further constraining the model parameters with the mass of $B_c(2S)$ newly measured by the CMS Collaboration. As important tasks of this work, the radiative transitions between the B_c states and the OZI-allowed two-body strong decays for the higher mass excited B_c states are evaluated with the wave functions obtained from the linear potential model. Our calculations may provide useful references to search for the excited B_c states. The main results are emphasized as follows.

For the S-wave states, the $2S$ hyperfine splitting is predicted to be $m[B_c^*(2S)] - m[B_c(2S)] \simeq 19$ MeV. The mass of the newly observed $B_c^*(2S)$ state might be determined via the $M1$ transition $B_c^*(2S) \to B_c\gamma$ in future experiments. The $3S$-wave states $B_c(3^1S_0)$ and $B_c(3^3S_1)$ are about 50 MeV above the DB^* threshold; their widths are estimated to be $\sim$100 MeV. Since production rates of the $3S$-wave B_c states in pp collisions at the LHC are comparable with those of the $2S$-wave B_c states [18], both $B_c(3^1S_0)$ and $B_c(3^3S_1)$ states may have large possibilities to be established in the DB^* final state, while $B_c(3^3S_1)$ might be observed in the DB final state as well.

For the P-wave states, it is found that the decays of the $2P$-wave states, $B_c(2^3P_0)$, $B_c(2P_1)$, and $B_c(2P'_1)$ together with all of the $1P$-wave states are governed by the $E1$ transitions; their typical decay widths are $\sim$100 keV. It should be possible to observe these P-wave states via their dominant radiative decay processes with the higher statistics of the LHC. The $B_c(2^3P_2)$ state is just $\sim$20 MeV above the DB threshold. It mainly decays into the DB channel with a very narrow width of $\Gamma \sim 1$ MeV, so it has a large potential to be first observed in the DB final state. The predicted masses of $3P$-wave states are in the range of (7420, 7470) MeV. They are broad states with widths of $\sim$200 MeV, and strongly couple to the B^*D^* final state. It is interesting to find that the $4P$-wave states $B_c(4^3P_0)$, $B_c(4P_1)$, and $B_c(4P'_1)$ with a mass around 7.7 GeV may have relatively narrow widths of $\mathcal{O}(100)$ MeV; these higher P-wave states might be first observed in their dominant channel DB or DB^*.

The $1D$-wave states mainly decay via the EM transitions. Our study indicates that these $1D$-wave states may have a relatively large potential to be observed via the radiative decay chains. For example, to look for the $B_c(1^3D_3)$ state, the $B_c(1^3D_3) \to B_c(1^3P_2)\gamma \to B_c(1^3S_1)\gamma\gamma \to B_c(1^1S_0)\gamma\gamma\gamma$ is worthy to be searched, for the branching fraction of this chain is estimated to be $\sim$100%. The masses of the $2D$ and $3D$ states are predicted to be $\sim$7.34 and 7.62 GeV, respectively. Their decays are governed by the strong decay modes, such as DB, DB^*, BD^*, or B^*D^*. These higher D-wave states usually have a width of $\mathcal{O}(100)$ MeV. The observations of the DB, DB^*, BD^*, or B^*D^* final states might be useful to search for these missing $2D$ and $3D$ states in future experiments.

For the F-wave states, one should pay more attention to $1F$-wave B_c states in future observations. They have a mass of $\sim$7.23 GeV and lie between the DB and B^*D mass thresholds. They are narrow states with a width of several MeV to several ten MeV, and dominantly decay into DB or B^*D channels. For example, the $B_c(1^3F_4)$ state might be a very narrow state with a width of $\sim$1 MeV; its decays are governed by the DB mode. To look for the missing $1F$-wave B_c states, the DB and B^*D final states are worth observing.

Finally, it should be pointed out the strong decay widths of the excited B_c states predicted in this work may have large uncertainties, for the parameter γ cannot be directly determined by the strong decay processes of B_c states. Fortunately, the uncertainties of the total strong decay widths of the excited B_c states do not affect the important information, such as the dominant decay modes and corresponding decay rates, for our searching for the excited B_c states in future experiments. Furthermore, the mixing angles for $^3P_1$–$^1P_1$, $^3D_2$–$^1D_2$, and $^3F_3$–$^1F_3$ have obvious model dependencies. The uncertainties of the mixing angles also affect our predictions of the decay properties of the mixed states.

ACKNOWLEDGMENTS

This work is supported by the National Natural Science Foundation of China under Grants No. 11775078, No. U1832173, No. 11705056, and No. 11405053.

[1] E. Eichten and F. Feinberg, Spin dependent forces in QCD, Phys. Rev. D **23**, 2724 (1981).
[2] F. Abe *et al.* (CDF Collaboration), Observation of B_c mesons in $p\bar{p}$ collisions at $\sqrt{s} = 1.8$ TeV, Phys. Rev. D **58**, 112004 (1998).
[3] G. Aad *et al.* (ATLAS Collaboration), Observation of an Excited $B_c^{\pm}$ Meson State with the ATLAS Detector, Phys. Rev. Lett. **113**, 212004 (2014).
[4] R. Aaij *et al.* (LHCb Collaboration), Search for excited B_c^+ states, J. High Energy Phys. 01 (2018) 138.
[5] A. M. Sirunyan *et al.* (CMS Collaboration), Observation of Two Excited B_c^+ States and Measurement of the $B_c^+(2S)$ Mass in pp Collisions at $\sqrt{s} = 13$ TeV, Phys. Rev. Lett. **122**, 132001 (2019).
[6] S. Godfrey and N. Isgur, Mesons in a relativized quark model with chromodynamics, Phys. Rev. D **32**, 189 (1985).
[7] E. J. Eichten and C. Quigg, Mesons with beauty and charm: Spectroscopy, Phys. Rev. D **49**, 5845 (1994).
[8] J. Zeng, J. W. Van Orden, and W. Roberts, Heavy mesons in a relativistic model, Phys. Rev. D **52**, 5229 (1995).
[9] V. V. Kiselev, A. K. Likhoded, and A. V. Tkabladze, B_c spectroscopy, Phys. Rev. D **51**, 3613 (1995).
[10] D. Ebert, R. N. Faustov, and V. O. Galkin, Properties of heavy quarkonia and B_c mesons in the relativistic quark model, Phys. Rev. D **67**, 014027 (2003).
[11] S. Godfrey, Spectroscopy of B_c mesons in the relativized quark model, Phys. Rev. D **70**, 054017 (2004).
[12] L. P. Fulcher, Phenomenological predictions of the properties of the B_c system, Phys. Rev. D **60**, 074006 (1999).
[13] A. Abd El-Hady, J. R. Spence, and J. P. Vary, Radiative decays of B_c mesons in a Bethe-Salpeter model, Phys. Rev. D **71**, 034006 (2005).
[14] N. Devlani, V. Kher, and A. K. Rai, Masses and electromagnetic transitions of the B_c mesons, Eur. Phys. J. A **50**, 154 (2014).
[15] A. P. Monteiro, M. Bhat, and K. B. Vijaya Kumar, Mass spectra and decays of ground and orbitally excited $c\bar{b}$ states in nonrelativistic quark model, Int. J. Mod. Phys. A **32**, 1750021 (2017).
[16] N. R. Soni, B. R. Joshi, R. P. Shah, H. R. Chauhan, and J. N. Pandya, $Q\bar{Q}$ $(Q \in \{b, c\})$ spectroscopy using the Cornell potential, Eur. Phys. J. C **78**, 592 (2018).
[17] A. P. Monteiro, M. Bhat, and K. B. Vijaya Kumar, $c\bar{b}$ spectrum and decay properties with coupled channel effects, Phys. Rev. D **95**, 054016 (2017).
[18] E. J. Eichten and C. Quigg, Mesons with beauty and charm: New horizons in spectroscopy, Phys. Rev. D **99**, 054025 (2019).
[19] M. Baldicchi and G. M. Prosperi, B_c meson and the light-heavy quarkonium spectrum, Phys. Rev. D **62**, 114024 (2000).
[20] S. Tang, Y. Li, P. Maris, and J. P. Vary, B_c mesons and their properties on the light front, Phys. Rev. D **98**, 114038 (2018).
[21] S. M. Ikhdair and R. Sever, B_c meson spectrum and hyperfine splittings in the shifted large N expansion technique, Int. J. Mod. Phys. A **18**, 4215 (2003).
[22] S. M. Ikhdair and R. Sever, Spectroscopy of B_c meson in a semirelativistic quark model using the shifted large N expansion method, Int. J. Mod. Phys. A **19**, 1771 (2004).
[23] D. M. Li, B. Ma, Y. X. Li, Q. K. Yao, and H. Yu, Meson spectrum in Regge phenomenology, Eur. Phys. J. C **37**, 323 (2004).
[24] K. W. Wei and X. H. Guo, Mass spectra of doubly heavy mesons in Regge phenomenology, Phys. Rev. D **81**, 076005 (2010).
[25] X. H. Guo, K. W. Wei, and X. H. Wu, Some mass relations for mesons and baryons in Regge phenomenology, Phys. Rev. D **78**, 056005 (2008).
[26] A. M. Badalian, B. L. G. Bakker, and I. V. Danilkin, The hyperfine splittings in bottomonium and the $B_q(q = n, s, c)$ mesons, Phys. Rev. D **81**, 071502 (2010); Erratum **81**, 099902(E) (2010).
[27] Z. G. Wang, Analysis of the vector and axialvector B_c mesons with QCD sum rules, Eur. Phys. J. A **49**, 131 (2013).
[28] W. Chen, Z. X. Cai, and S. L. Zhu, Masses of the tensor mesons with $J^P = 2^-$, Nucl. Phys. **B887**, 201 (2014).
[29] A. K. Rai, B. Patel, and P. C. Vinodkumar, Properties of $Q\bar{Q}$ mesons in non-relativistic QCD formalism, Phys. Rev. C **78**, 055202 (2008).
[30] B. Patel and P. C. Vinodkumar, Properties of $Q\bar{Q}(Q \in b, c)$ mesons in Coulomb plus Power potential, J. Phys. G **36**, 035003 (2009).
[31] A. Bernotas and V. Simonis, Heavy hadron spectroscopy and the bag model, Lith. J. Phys. **49**, 19 (2009).
[32] S. M. Ikhdair and R. Sever, B_c and heavy meson spectroscopy in the local approximation of the Schrodinger equation with relativistic kinematics, Int. J. Mod. Phys. A **20**, 4035 (2005).
[33] A. Abd El-Hady, M. A. K. Lodhi, and J. P. Vary, B_c mesons in a Bethe-Salpeter model, Phys. Rev. D **59**, 094001 (1999).
[34] L. Motyka and K. Zalewski, Mass spectra and leptonic decay widths of heavy quarkonia, Eur. Phys. J. C **4**, 107 (1998).
[35] C. T. H. Davies, K. Hornbostel, G. P. Lepage, A. J. Lidsey, J. Shigemitsu, and J. H. Sloan, B(c) spectroscopy from lattice QCD, Phys. Lett. B **382**, 131 (1996).
[36] N. Mathur, M. Padmanath, and S. Mondal, Precise Predictions of Charmed-Bottom Hadrons from Lattice QCD, Phys. Rev. Lett. **121**, 202002 (2018).
[37] R. J. Dowdall, C. T. H. Davies, T. C. Hammant, and R. R. Horgan, Precise heavy-light meson masses and hyperfine splittings from lattice QCD including charm quarks in the sea, Phys. Rev. D **86**, 094510 (2012).
[38] E. B. Gregory, C. T. H. Davies, E. Follana, E. Gamiz, I. D. Kendall, G. P. Lepage, H. Na, J. Shigemitsu, and K. Y. Wong, A Prediction of the B_c^* Mass in Full Lattice QCD, Phys. Rev. Lett. **104**, 022001 (2010).
[39] I. F. Allison, C. T. H. Davies, A. Gray, A. S. Kronfeld, P. B. Mackenzie, and J. N. Simone (HPQCD, Fermilab Lattice, and UKQCD Collaborations), Mass of the B_c Meson in Three-Flavor Lattice QCD, Phys. Rev. Lett. **94**, 172001 (2005).
[40] K. M. Cheung, B_c Mesons Production at Hadron Colliders by Heavy Quark Fragmentation, Phys. Rev. Lett. **71**, 3413 (1993).
[41] E. Braaten, S. Fleming, and T. C. Yuan, Production of heavy quarkonium in high-energy colliders, Annu. Rev. Nucl. Part. Sci. **46**, 197 (1996).

[42] K. M. Cheung and T. C. Yuan, Heavy quark fragmentation functions for d wave quarkonium and charmed beauty mesons, Phys. Rev. D **53**, 3591 (1996).

[43] K. M. Cheung and T. C. Yuan, Hadronic production of S wave and P wave charmed beauty mesons via heavy quark fragmentation, Phys. Rev. D **53**, 1232 (1996).

[44] A. V. Berezhnoy, V. V. Kiselev, and A. K. Likhoded, Hadronic production of S and P wave states of $\bar{b}c$ quarkonium, Z. Phys. A **356**, 79 (1996).

[45] C. H. Chang, J. X. Wang, and X. G. Wu, Hadronic production of the P-wave excited B_c -states $B^*_{cJ,L=1}$, Phys. Rev. D **70**, 114019 (2004).

[46] C. H. Chang, C. F. Qiao, J. X. Wang, and X. G. Wu, The Color-octet contributions to P-wave B_c meson hadroproduction, Phys. Rev. D **71**, 074012 (2005).

[47] Q. L. Liao, Y. Deng, Y. Yu, G. C. Wang, and G. Y. Xie, Heavy P-wave quarkonium production via Higgs decays, Phys. Rev. D **98**, 036014 (2018).

[48] K. He, H. Y. Bi, R. Y. Zhang, X. Z. Li, and W. G. Ma, P-wave excited B_c^{**} meson photoproduction at the LHeC, J. Phys. G **45**, 055005 (2018).

[49] Q. L. Liao, Y. Yu, Y. Deng, G. Y. Xie, and G. C. Wang, Excited heavy quarkonium production via Z^0 decays at a high luminosity collider, Phys. Rev. D **91**, 114030 (2015).

[50] Q. L. Liao and G. Y. Xie, Heavy quarkonium wave functions at the origin and excited heavy quarkonium production via top quark decays at the LHC, Phys. Rev. D **90**, 054007 (2014).

[51] Q. L. Liao, X. G. Wu, J. Jiang, Z. Yang, and Z. Y. Fang, Heavy quarkonium production at LHC through W boson decays, Phys. Rev. D **85**, 014032 (2012).

[52] Z. Yang, X. G. Wu, L. C. Deng, J. W. Zhang, and G. Chen, Production of the P-wave excited B_c-states through the Z^0 boson decays, Eur. Phys. J. C **71**, 1563 (2011).

[53] C. H. Chang, J. X. Wang, and X. G. Wu, Production of B_c or $\bar{B}_c$ meson and its excited states via $\bar{t}$ quark or t quark decays, Phys. Rev. D **77**, 014022 (2008).

[54] S. Patnaik, P. C. Dash, S. Kar, S. Patra, and N. Barik, Magnetic dipole transitions of B_c and B_c^* mesons in the relativistic independent quark model, Phys. Rev. D **96**, 116010 (2017); Erratum **99**, 019901(E) (2019).

[55] V. Simonis, Magnetic properties of ground-state mesons, Eur. Phys. J. A **52**, 90 (2016).

[56] T. Wang, Y. Jiang, W. L. Ju, H. Yuan, and G. L. Wang, The electromagnetic decays of $B_c(2S)$, J. High Energy Phys. 03 (2016) 209.

[57] Z. G. Wang, The radiative decays $B_c^{*\pm} \to B_c^{\pm}\gamma$ with QCD sum rules, Eur. Phys. J. C **73**, 2559 (2013).

[58] D. Ebert, R. N. Faustov, and V. O. Galkin, Radiative M1 decays of heavy light mesons in the relativistic quark model, Phys. Lett. B **537**, 241 (2002).

[59] J. Ferretti and E. Santopinto, Open-flavor strong decays of open-charm and open-bottom mesons in the $^3P_0$ model, Phys. Rev. D **97**, 114020 (2018).

[60] V. V. Kiselev, Decay of $B_c^{*+}(3S) \to B^+ D^0$, Phys. Lett. B **390**, 427 (1997).

[61] W. J. Deng, H. Liu, L. C. Gui, and X. H. Zhong, Charmonium spectrum and their electromagnetic transitions with higher multipole contributions, Phys. Rev. D **95**, 034026 (2017).

[62] W. J. Deng, H. Liu, L. C. Gui, and X. H. Zhong, Spectrum and electromagnetic transitions of bottomonium, Phys. Rev. D **95**, 074002 (2017).

[63] L. Micu, Decay rates of meson resonances in a quark model, Nucl. Phys. **B10**, 521 (1969).

[64] A. Le Yaouanc, L. Oliver, O. Pene, and J. C. Raynal, Naive quark pair creation model of strong interaction vertices, Phys. Rev. D **8**, 2223 (1973).

[65] A. Le Yaouanc, L. Oliver, O. Pene, and J.-C. Raynal, Naive quark pair creation model and baryon decays, Phys. Rev. D **9**, 1415 (1974).

[66] T. Barnes, S. Godfrey, and E. S. Swanson, Higher charmonia, Phys. Rev. D **72**, 054026 (2005).

[67] C. H. Cai and L. Li, Radial equation of bound state and binding energies of Ξ^- hypernuclei, Chin. Phys. C **27**, 1005 (2003).

[68] L. Y. Xiao, K. L. Wang, Q. F. Lü, X. H. Zhong, and S. L. Zhu, Strong and radiative decays of the doubly charmed baryons, Phys. Rev. D **96**, 094005 (2017).

[69] K. L. Wang, L. Y. Xiao, X. H. Zhong, and Q. Zhao, Understanding the newly observed Ω_c states through their decays, Phys. Rev. D **95**, 116010 (2017).

[70] Q. F. Lü, K. L. Wang, L. Y. Xiao, and X. H. Zhong, Mass spectra and radiative transitions of doubly heavy baryons in a relativized quark model, Phys. Rev. D **96**, 114006 (2017).

[71] K. L. Wang, Y. X. Yao, X. H. Zhong, and Q. Zhao, Strong and radiative decays of the low-lying S- and P-wave singly heavy baryons, Phys. Rev. D **96**, 116016 (2017).

[72] Y. X. Yao, K. L. Wang, and X. H. Zhong, Strong and radiative decays of the low-lying D-wave singly heavy baryons, Phys. Rev. D **98**, 076015 (2018).

[73] S. J. Brodsky and J. R. Primack, The Electromagnetic interactions of composite systems, Ann. Phys. (N.Y.) **52**, 315 (1969).

[74] Z. P. Li, H. X. Ye, and M. H. Lu, A unified approach to pseudoscalar meson photoproductions off nucleons in the quark model, Phys. Rev. C **56**, 1099 (1997).

[75] Q. Zhao, J. S. Al-Khalili, Z. P. Li, and R. L. Workman, Pion photoproduction on the nucleon in the quark model, Phys. Rev. C **65**, 065204 (2002).

[76] L. Y. Xiao, X. Cao, and X. H. Zhong, Neutral pion photoproduction on the nucleon in a chiral quark model, Phys. Rev. C **92**, 035202 (2015).

[77] X. H. Zhong and Q. Zhao, η photoproduction on the quasi-free nucleons in the chiral quark model, Phys. Rev. C **84**, 045207 (2011).

[78] X. H. Zhong and Q. Zhao, η' photoproduction on the nucleons in the quark model, Phys. Rev. C **84**, 065204 (2011).

[79] M. Jacob and G. C. Wick, On the general theory of collisions for particles with spin, Ann. Phys. (N.Y.) **7**, 404 (1959); **281**, 774 (2000).

[80] L. C. Gui, L. S. Lu, Q. F. Lü, X. H. Zhong, and Q. Zhao, Strong decays of higher charmonium states into open-charm meson pairs, Phys. Rev. D **98**, 016010 (2018).

[81] Q. F. Lü, T. T. Pan, Y. Y. Wang, E. Wang, and D. M. Li, Excited bottom and bottom-strange mesons in the quark model, Phys. Rev. D **94**, 074012 (2016).

[82] D. M. Li, P. F. Ji, and B. Ma, The newly observed open-charm states in quark model, Eur. Phys. J. C **71**, 1582 (2011).

[83] M. Tanabashi *et al.* (Particle Data Group), Review of particle physics, Phys. Rev. D **98**, 030001 (2018).
[84] E. S. Ackleh, T. Barnes, and E. S. Swanson, On the mechanism of open flavor strong decays, Phys. Rev. D **54**, 6811 (1996).
[85] T. Barnes, N. Black, and P. R. Page, Strong decays of strange quarkonia, Phys. Rev. D **68**, 054014 (2003).
[86] S. Godfrey, K. Moats, and E. S. Swanson, B and B_s Meson Spectroscopy, Phys. Rev. D **94**, 054025 (2016).
[87] S. Godfrey and K. Moats, Properties of excited charm and charm-strange mesons, Phys. Rev. D **93**, 034035 (2016).
[88] F. E. Close and E. S. Swanson, Dynamics and decay of heavy-light hadrons, Phys. Rev. D **72**, 094004 (2005).